IV International Conference on Particle-based Methods – Fundamentals and Applications
PARTICLES 2015
E. Oñate, M. Bischoff, D.R.J. Owen, P. Wriggers & T. Zohdi (Eds)

FROM ELASTO-PLASTICITY TO VISCO-ELASTO-PLASTICITY FOR SATURATED GRANULAR MATERIALS

BRUNO CHAREYRE[1], DONIA MARZOUGUI[1], JULIEN CHAUCHAT[2]

[1]3SR, Univ. Grenoble Alpes, F-38000 Grenoble, France and
3SR, CNRS, F-38000 Grenoble, France
[2]LEGI, Univ. Grenoble Alpes, F-38000 Grenoble, France and
LEGI, CNRS, F-38000 Grenoble, France

Key words: Granular Materials, Lubrication, Poromechanics, Suspension, Viscoplasticity

Abstract. A recent extension of the discrete element method is reported for the simulation of dense mixtures of non-colloidal particles and viscous fluids in the non-inertial regime. The numerical model includes sphere-sphere contacts using a soft contact approach [2], short range hydrodynamic interactions defined by frame-invariant expressions of forces and torques in the lubrication approximation, and drag forces resulting from the poromechanical coupling computed with the DEM-PFV technique [3]. The proposed model is general and applies directly to sheared satured granular media in which pore pressure feedback plays a key role. A partitioned solver makes the algorithm trivially parallel, which enables the coupled problems to be solved with nearly the same wall-clock time as uncoupled dry materials simulations. The shear stress in a dense suspension is analyzed, and decomposed into contact stress and hydrodynamic stress. Both contributions are shown to be increasing functions of a dimensionless shear rate Iv, in agreement with experimental results [4]. In contrast with a popular idea, the results suggest that lubrication may not necessarily reduce the contribution of contact forces to the bulk shear stress.

1 INTRODUCTION

Simulating the flow of saturated granular materials raises two challenging questions: 1) how to reflect the rheological properties of the moving materials in relevant constitutive laws and, 2) how to solve a boundary value problem when this constitutive law is used combined with very large deformations and a complex morphology of the run-out slope. Advances are needed on both points in order to provide the engineers with better tools, enabling namely numerical studies of gravitational flows from the triggering to the possible impact on structures and infrastructures.

Regarding the second question, the conventional FEM methods are helpless due to (namely) the moving free surface of the flow. The methods usually used for fluid dynamics (such as direct Navier-Stokes solvers or the Lattice-Boltzman method) may have less problems with the free surface but they make the implementation of complex visco-elasto-plastic models extremely difficult. To overcome these difficulties dedicated techniques have been developed in the recent years, using e.g. the SPH[10] (Smoothed Particle Hydrodynamics) or the FEMLIP[5] (FEM with lagrangian integration points). In this paper we focus on the first question: the rheology of flowing geomaterials, and we propose an approach of this question through micromechanical modeling as in [9]. Recent developments of the discrete element method (DEM) are explained in the first section and the results of simulated simple shear tests are summarized.

2 MICROMECHANICAL MODEL OF PARTICLES IN A VISCOUS FLUID

We assume that the flowing material can be conceptualized as a granular material. This assumption is relevant for the grain size of silts and above. Clayey materials (i.e. colloidal particles) are very different and exhibit much more complex interactions between particles, thus this study does not consider pure clays. For the mixtures of clay and coarser particles, the present approach may be valid as soon as the clay content and the pore water can be accounted for altogether as an equivalent viscous suspension carrying the bigger particles. Hereafter we introduce a numerical coupling between the DEM and a hydrodynamic model.

2.1 Discrete Element Model

An explicit finite difference scheme is employed for updating the position of each particle in a time-marching algorithm. The particles move according to the Newton's second law. The interactions between particles are governed by elastic-frictional contact forces defined using a soft contact approach [4]. The contact parameters are the normal and shear stiffnesses k_n and k_s, and the angle of contact friction ϕ. The contact forces are supplemented hereafter with forces coming from the interstitial fluid. A three-dimensional implementation of the DEM as found in the open source software YADE is used herein. For more details about the implementation, please refer to [13].

2.2 Long range interactions

The DEM-PFV method is used to solve a pore-scale version of the mass balance equation which appears in the continuous theory of porous media and leads to the so-called poromechanical coupling - leading to long range interactions between the particles. Only the main steps of the method are outlined hereafter since the details can be found in previous papers. We assume incompressible phases as in [3, 2] (for compressible phases see [11]). A tetrahedral decomposition of the pore space is introduced based on regular triangulation (figure 1), where that part of a tetrahedron occupied by the fluid is called

a *pore*. From now on V_i denotes the volume of pore i. It is uniquely defined by the positions $\mathbf{x}_i$ and sizes of the solid particles, while the rate of change $\dot{V}_i$ also depends on their velocities $\dot{\mathbf{x}}_i$.

An exchange of fluid between adjacent pores i and j is represented by the interface flux q_{ij}. The volume balance equation gives

$$\dot{V}_i \ = \ \sum_{j=1}^{j=4} q_{ij}. \tag{1}$$

A linear relationship between q_{ij} and the local pressure gradient $(p_i - p_j)/l_{ij}$ (where l_{ij} is a reference length [3]) leads to

$$\dot{V}_i = \ \sum_{j=1}^{j=4} k_{ij} \ (p_j - p_i)/l_{ij} = \ \sum_{j=1}^{j=4} K_{ij} \ (p_j - p_i). \tag{2}$$

In this equation K_{ij} is the local hydraulic conductivity. It reflects the small scale geometry of the packing. In details, the proposed expression of K_{ij} depends on a local hydraulic radius R^h_{ij} (area of the fluid-solid interface divided by the fluid volume - again see [3]) as

$$K_{ij} = \alpha \frac{S^f_{ij} {R^h_{ij}}^2}{2\eta \, l_{ij}} \tag{3}$$

where S^f_{ij} is the cross-sectional area of the pore-throat, η is the viscosity of the fluid, and α can be interpreted as a calibration parameter. $\alpha = 1$ is known to give good estimates of the actual permeability of glass beads [14] but we used $\alpha < 1$ in this study. This is further discussed in section 3.

Substituting $\dot{V}_i$ by its expression in terms of particles velocity and writing equation 2 for every element gives a system of linear equations. At each time step in the motion integration, solving this system gives a discrete field of fluid pressure $\mathbf{P}$ as function of the particles velocity.

The drag forces are deduced from the pressure field. They are the integrals of the pressure p and the viscous stress τ on the surface of the particle, i.e.

$$F^f_k = \int_{\partial\Gamma_k} p\mathbf{n}ds + \int_{\partial\Gamma_k} \tau\mathbf{n}ds \tag{4}$$

The F^f_k are introduced in Newton's second law together with the forces coming from solid contacts ($\mathbf{F}^c$) and lubrication effects ($\mathbf{F}^L$ defined in the next section). I.e.

$$\mathbf{M}\ddot{\mathbf{x}} = \mathbf{F}^c + \mathbf{F}^L + \mathbf{F}^f, \tag{5}$$

The strong two-way coupling defined by equation 5 (remember that $\mathbf{F}^f$ depends on $\dot{\mathbf{x}}$) is the poromechanical coupling. It is integrated with an explicit scheme whose accuracy has been verified in [2].

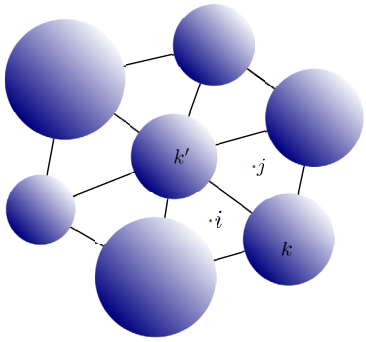

Figure 1: Regular triangulation in 2D.

2.3 Short range interactions

The lubrication forces are linked to the presence of the fluid and are only significant for nearly touching particles. We note particles k and k' with radii a_k and $a_{k'}$, linear velocities $\boldsymbol{v}_k$ and $\boldsymbol{v}_{k'}$ and angular velocities $\boldsymbol{\omega}_k$ and $\boldsymbol{\omega}_{k'}$, respectively. Their average radius is defined as $a = (a_k + a_{k'})/2$ and h denotes the inter-particle distance (surface to surface). An arbitrary relative motion between two particles can be decomposed in four elementary motions corresponding to normal displacement (subscript n), shear displacement (s), rolling (r) and twisting (t). For full details see [9]. Noting $\boldsymbol{\omega}_n = (\boldsymbol{v}_{k'} - \boldsymbol{v}_k) \times \mathbf{n} / (a_k + a_{k'} + h)$ the angular velocity of the local frame attached to the interacting pair, lubrication forces and torques are defined as follow:

$$\boldsymbol{F}_n^L = \frac{3}{2}\,\pi\,\eta\,\frac{a^2}{h}\,\mathbf{v}_n \tag{6}$$

$$\boldsymbol{F}_s^L = \frac{\pi\eta}{2}\left[-2a + (2a+h)\,ln\left(\frac{2a+h}{h}\right)\right]\,\mathbf{v}_t \tag{7}$$

$$\boldsymbol{C}_r^L = \pi\,\eta\,a^3\left(\frac{3}{2}\,ln\frac{a}{h} + \frac{63}{500}\,\frac{h}{a}\,ln\frac{a}{h}\right)\,[(\boldsymbol{\omega}_k - \boldsymbol{\omega}_{k'}) \times \mathbf{n}] \tag{8}$$

$$\boldsymbol{C}_t^L = \pi\,\eta\,a^2\,\frac{h}{a}\,ln\frac{a}{h}\,[(\boldsymbol{\omega}_k - \boldsymbol{\omega}_{k'}) \cdot \mathbf{n}]\,\mathbf{n} \tag{9}$$

where $\mathbf{v}_n = ((\mathbf{v}_{k'} - \mathbf{v}_k) \cdot \mathbf{n})\,\mathbf{n}$ is the normal relative velocity and $\mathbf{v}_t = (a_k(\boldsymbol{\omega}_k - \boldsymbol{\omega}_n) + a_{k'}(\boldsymbol{\omega}_{k'} - \boldsymbol{\omega}_n)) \times \mathbf{n}$ is an objective expression of the tangential relative velocity. In this set of equations, the normal and shear forces, $\boldsymbol{F}_n$ and $\boldsymbol{F}_s$, are based on Frankel & Acrivos [6, 15] whereas C_r and C_t are based on Jeffrey & Onishi [8, 7]. The total lubrication force $\boldsymbol{F}_k^L$ (resp. $\boldsymbol{F}_{k'}^L$) applied by particle k' on particle k (resp. by particle k on particle k') and the total torque $\boldsymbol{C}_k^L$ (resp. $\boldsymbol{C}_{k'}^L$) applied by particle k' on particle k (resp. by particle k on particle k') relative to the particle center read:

$$\boldsymbol{F}_k^L \;=\; -\boldsymbol{F}_{k'}^L \;=\; \boldsymbol{F}_n \;+\; \boldsymbol{F}_s, \tag{10}$$

$$\boldsymbol{C}_k^L \;=\; (a_k + \frac{h}{2})\,\boldsymbol{F}_s + \;\boldsymbol{C}_r + \;\boldsymbol{C}_t, \tag{11}$$

$$\boldsymbol{C}_{k'}^L \;=\; (a_{k'} + \frac{h}{2})\,\boldsymbol{F}_s - \;\boldsymbol{C}_r - \;\boldsymbol{C}_t. \tag{12}$$

We account for the deformability of the particles near the contact region by combining the above normal lubrication model with the linear contact model via a Maxwell-type visco-elastic scheme ([9]. Lastly, we introduce a surface roughness such that the contact model and the lubrication model use slightly different values of h. The repulsive contact force appears even before $h = 0$ so that practically $h \leq 0$ never occurs in simulations.

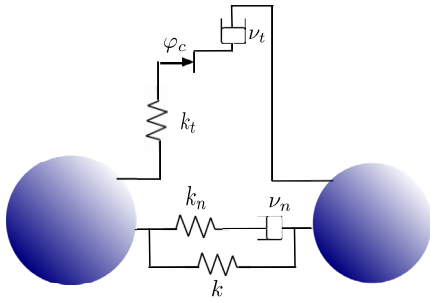

Figure 2: Visco-elastic scheme of the interaction between two elastic-like particles.

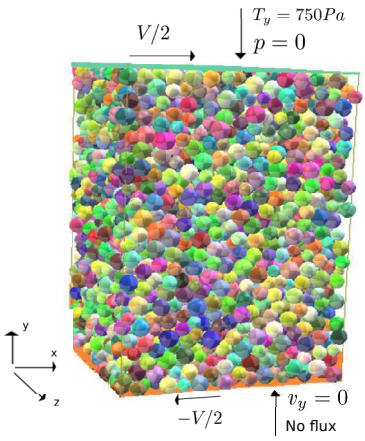

Figure 3: Simulation cell.

2.4 A note on computational cost

The time integration is done using a partitioned approach. At each step the contribution of contact forces and the fluid forces are summed, and the total force is used to update momentum using a classical (explicit) centered finite difference scheme. A purely sequential vision of this procedure is shown in figure 4(a). Both types of forces are uniquely defined by the positions and velocities of the previous step. It makes the algorithm pleasantly parallel, as contact interactions and fluid forces (including lubrication forces) can be computed simultaneously (fig. 4(b)). Virtually, it results in a fluid model which comes at no cost compared to the classical DEM without fluid. This is assuming that the computational resources are not limited and that the overhead coming from summing the fluid forces and the contact forces is negligible (practically it is). There is of course no restriction on how each branch in fig. 4(b) is further parallelized.

How close to this theoretical performance a concrete implementation can be depends on many factors. Namely, the performance of the original DEM code is a key factor. Indeed there is no merit in computing fluid forces faster than contact forces if the latest is initially slow. Also, the number of particles plays a role since the computational cost of contacts and fluid solver may scale differently (the fluid solver has to solve a sparse linear system). Our tests with the YADE-DEM code used in this study showed that assigning four cores to both the contact and the fluid parts leads to an increase of the computation time of the order of 50% for a range of problem sizes between 5,000 and 20,000 particles. Below 5,000, the cost of the fluid is almost negligible. Above 20,000 particles the fluid solver tend dominate the computation time. Further investigations will be done on this question.

3 SIMPLE SHEAR AT IMPOSED NORMAL PRESSURE

We simulate a saturated flowing material with bi-periodic boundary conditions, made of $N = 1000$ frictional spheres of average radius $a = 0.025 \pm 0.01$ m. The physical properties are roughness $\varepsilon = 0.035\,a$, density $\rho = 2500$ kg/m^3, normal contact stiffness $k_n/a = 5 \times 10^5$ Pa, shear stiffness $k_s = k_n/2$, and contact friction angle $\varphi = 30°$. There is no gravity. The numerical sample is first confined between two parallel plates then sheared by moving the top and the bottom plates at constant velocity $\pm V/2 = 1.5$ m/s. The boundary conditions for the top plate are the velocities $v_x = V/2$, $v_z = 0$, the total normal stress $T_y = 750$ Pa and the fluid pressure $p = 0$. At the bottom plate, $v_x = -V/2$, $v_z = 0$ and the fluid velocity along the y axis $v_y^f = 0$ (impermeable boundary). Periodic boundary conditions are defined along the horizontal axis for both the particles and the fluid. The external stress vector is $\boldsymbol{T} = \boldsymbol{F}/S$ where $\boldsymbol{F}$ is the total force on the top plate and S is the horizontal cross sectional area. T_y is kept constant during the deformation, while T_x is a result of the imposed shear.

Figure 6 shows the evolution of the shear stress T_x, the pressure p and the solid fraction ϕ function of the deformation $\gamma(T) = \int_0^T \dot{\gamma}(t)dt$ where $\dot{\gamma}(t) = V/H(t)$ is the shear rate.

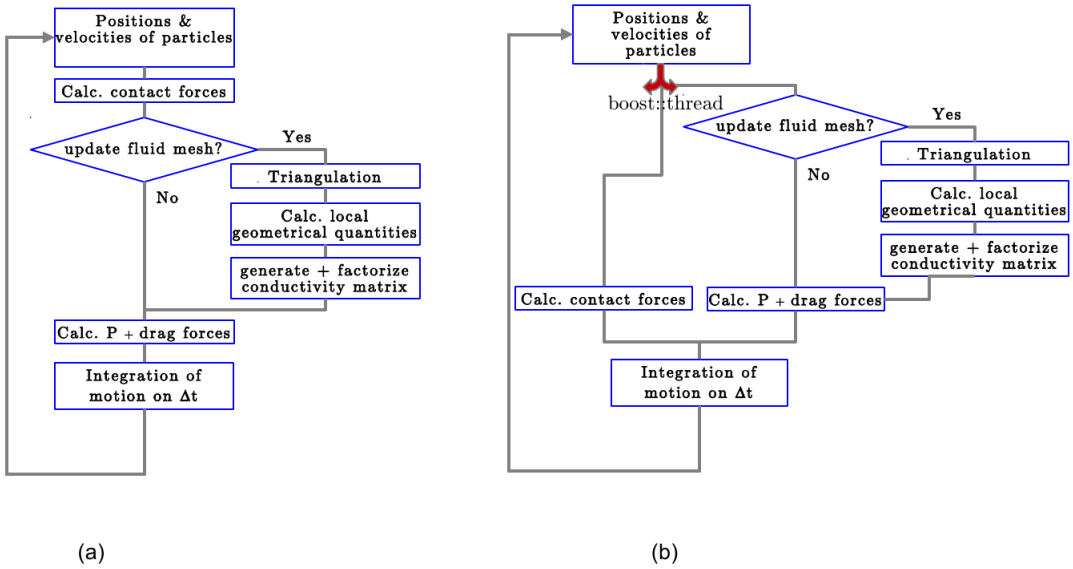

Figure 4: The time-stepping algorithm for the coupled problems, (a) purely sequential or (b) using task parallelism.

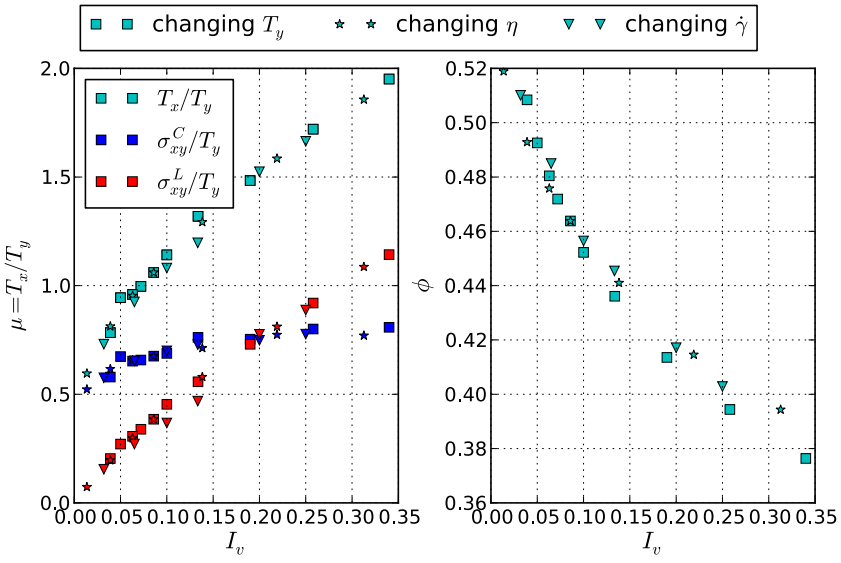

Figure 5: Normalized shear stress and solid fraction at steady state versus I_v. In each series the change of I_v is obtained by changing a different parameter: normal stress, viscosity, or shear rate.

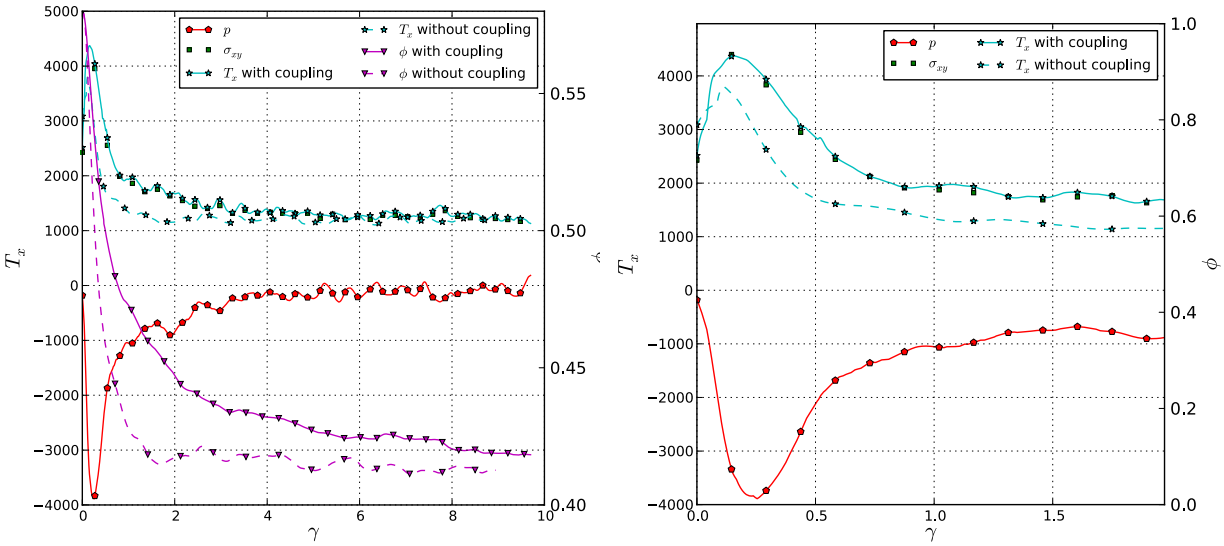

Figure 6: (left): The evolution of the shear stress and the solid fraction as a function of the deformation, with and without the poromechanical coupling. (right): Zoom on the transient regime.

The numerical results are presented for two cases: a first case where the poromechanical coupling (long range interactions) is included and another one where it is not (i.e. ignoring the last term in equation 5). In the early stage of deformation a transient regime is observed, reminiscent of the critical state theory. It is characterized by a peak stress, a decrease of the solid fraction and a negative pore pressure in the coupled case. This later effect entails a higher effective stress in the coupled problem, explaining why the shear stress reaches higher values. The system evolves toward a steady state for large deformations, in which the shear stress and the solid fraction are approximately constant and the pore pressure is nearly zero. The poromechanical coupling has no visible effect at steady state: the shear stress and the solid fraction reach similar values for both cases.

At steady state in non-inertial regimes the stress ratio $\mu = T_x/T_y$ and the solid fraction ϕ are entirely controlled by the viscous number I_v. I_v is a dimensionless form of the shear rate [1], reflecting the magnitude of viscous effects, and is defined as:

$$I_v = \frac{\eta \left|\dot{\gamma}\right|}{T_y}, \tag{13}$$

In other words, all possible combinations of confining pressure, fluid viscosity, and shear rate corresponding to a given value of I_v give the same result. It is easily confirmed by comparing simulations in which these control parameters are changed independently to produce different values of I_v (fig. 5).

Finally, a validation of our coupled model is obtained by comparing the normalized shear stress and the solid fraction at steady state with the empirical equation of [1] (fig. 7, the empirical relation is plotted for convenience, it goes through data points not shown in the figure).

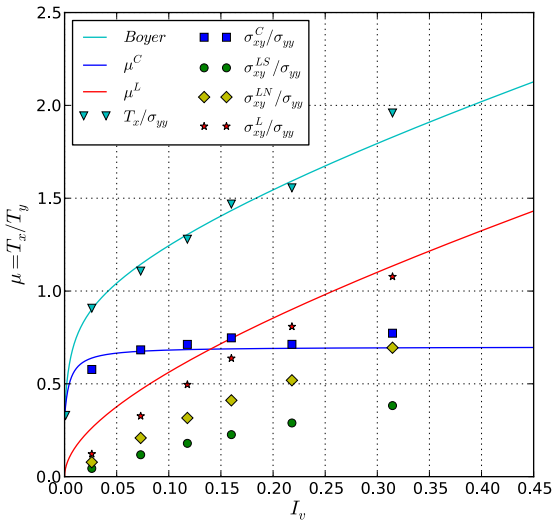

Figure 7: The stress ratio μ and the decomposition in contact stress, normal lubrication stress and shear lubrication stress. The solid line is the phenomenological law of [1].

4 DISCUSSION

The previous section reveals a key feature of saturated geomaterials which has implications on debris flow: the shear stress and the solid fraction (or porosity) at large deformations are no longer uniquely defined by the confining stress as in critical state theory. They are both dependent on the shear rate. The effect is relatively well known as an experimental fact in the rheology of suspensions. It is attributed to the short range lubrication effects.

A consequence rarely discussed, however, is that the rate dependent volume changes are strongly coupled with long range poromechanical effects. In rheometer tests, the shear rate is usually applied for a sufficiently long time period so that the measurements are done at steady state. The transient regime is disregarded and the pore pressure is not recorded in most cases. For debris flow in natural conditions however, the shear rate may not be constant if the material is flowing down a slope where the slope angle is not constant. In such case the flowing material may never reach the steady state and it may be strongly influenced by the pore pressure changes associated to the poromechanical coupling.

Let us recall that the poromechanical coupling entails long range effects in the system and, ultimately, a dependency on the problem size. Indeed the characteristic time of poromechanical effects scale with $\eta H^2/\kappa$ where κ is the intrinsic permeability and the problem size. Since κ scales with a^2 (squared particle size), the relaxation time of the transient regime is proportional to $\eta(H/a)^2$. A consequence is that the peak pore pressure and the peak stress in figure 6 scales with $(H/a)^2$. That is, they are much more significant

in large scale in-situ conditions than in small scale lab tests.

A key conclusion is that it is impossible to modelize a flowing suspension as an equivalent single-phase mixture. It is always necessary to solve a coupled problem. Promising steps in this direction can be found in [10], which provides an efficient computational techniques at the field scale. The micromechanical model we presented in this paper is complementary, in the sense that it hardly applies to large scale problems but it can provide insight into the rheology of the flowing materials and the coupling phenomena. It is freely available as part of Yade-DEM [12] and it can be used for further investigations.

References

REFERENCES

[1] Boyer, F., Guazzelli, E., and Pouliquen, O. Unifying suspension and granular rheology. *Physical Review Letters 107*, 18 (2011), 188301.

[2] Catalano, E., Chareyre, B., and Barthélémy, E. Pore-scale modeling of fluid-particles interaction and emerging poromechanical effects. *International Journal for Numerical and Analytical Methods in Geomechanics 38*, 1 (2014), 51–71.

[3] Chareyre, B., Cortis, A., Catalano, E., and Barthélemy, E. Pore-scale modeling of viscous flow and induced forces in dense sphere packings. *Transport in porous media 94*, 2 (2012), 595–615.

[4] Cundall, P., and Strack, O. A discrete numerical model for granular assemblies. *Geotechnique 29*, 1 (1979), 47–65.

[5] Cuomo, S., Prime, N., Iannone, A., Dufour, F., Cascini, L., and Darve, F. Large deformation femlip drained analysis of a vertical cut. *Acta Geotechnica 8*, 2 (2013), 125–136.

[6] Frankel, N., and Acrivos, A. On the viscosity of a concentrated suspension of solid spheres. *Chemical Engineering Science 22*, 6 (1967), 847853.

[7] Jeffrey, D., and Onishi, Y. Calculation of the resistance and mobility functions for two unequal rigid spheres in low-reynolds-number flow. *Journal of Fluid Mechanics 139* (1984), 261–290.

[8] Jeffrey, D., and Onishi, Y. The forces and couples acting on two nearly touching spheres in low-reynolds-number flow. *Zeitschrift für angewandte Mathematik und Physik ZAMP 35*, 5 (1984), 634–641.

[9] Marzougui, D., Chareyre, B., and Chauchat, J. Microscopic origins of shear stress in dense fluid–grain mixtures. *Granular Matter* (2015), DOI:10.1007/s10035–015–0560–6.

[10] Pastor, M., Blanc, T., Haddad, B., Drempetic, V., Morles, M., Dutto, P., Stickle, M., Mira, P., and Merodo, J. Depth averaged models for fast landslide propagation: Mathematical, rheological and numerical aspects. *Archives of Computational Methods in Engineering 22*, 1 (2015), 67–104.

[11] Scholtès, L., Chareyre, B., Michallet, H., Catalano, E., and Marzougui, D. Modeling wave-induced pore pressure and effective stress in a granular seabed. *Continuum Mechanics and Thermodynamics 27*, 1-2 (2015), 305–323.

[12] Smilauer, V., Catalano, E., Chareyre, B., Dorofenko, S., Duriez, J., Gladky, A., Kozicki, J., Modenese, C., Scholtès, L., Sibille, L., Stransky, J., and Thoeni, K. Yade Reference Documentation. In *Yade Documentation*, V. Smilauer, Ed., 1st ed. The Yade Project, 2010. http://yade-dem.org/doc/.

[13] Smilauer, V., and Chareyre, B. Yade Dem Formulation. In *Yade Documentation*, V. Smilauer, Ed., 1st ed. The Yade Project, 2010. http://yade-dem.org/doc/.

[14] Tong, A.-T., Catalano, E., and Chareyre, B. Pore-Scale Flow Simulations: Model Predictions Compared with Experiments on Bi-Dispersed Granular Assemblies. *Oil & Gas Science and Technology-Revue d'IFP Energies Nouvelles 67*, 5 (2012), 743–752.

[15] Van den Brule, B., and Jongschaap, R. Modeling of concentrated suspensions. *Journal of statistical physics 62*, 5 (1991), 12251237.